Confocal Bistatic LIDAR in Scattering Media

Justin Folden[a], Derek Alley[b], David Illig[b], Linda Mullen[b], and Sanjeev J. Koppal[a]

[a]Electrical and Computer Engineering, University of Florida, Gainesville, FL 32611
[b]U.S. Navy NAWCAD Patuxent River, MD 20670

ABSTRACT

Scattering effects in underwater environments significantly challenge optical perception. This paper introduces a foveating confocal bistatic LiDAR system, uniquely capable of adaptive targeting with its MEMS-modulated transmitter and receiver in turbid underwater conditions. By dynamically adjusting its receiver instantaneous field of view to areas of interest, it effectively increases depth sampling in complex and challenging underwater environments. Applying bistatic principles, separating transmitter and receiver, we allow robustness to scattering media effects. We demonstrate LIDAR results in an underwater laboratory tank setting.

1. INTRODUCTION

LiDAR sensors are critical in diverse depth sensing applications but face challenges in turbid underwater environments due to scattering effects. To address this, our work introduces a foveating confocal bistatic LiDAR system, inspired by automobile fog lights.

We present two major contributions:

- Introduction of a novel underwater bistatic LiDAR system employing MEMS mirror modulation for both transmitter and receiver. Our optical setup separates the illumination source from the receiver to diminish backscatter, a concept reflected in.[1]
- Development and testing of a prototype in a laboratory tank setting, validating our design and models with real-world data. This enables a technique to control sensor sampling density at different depths, we term as *foveation* of the LIDAR.

2. RELATED WORK

Time-of-Flight (TOF) Imaging and Adaptive Optics: In contrast to using fast adaptive optics for atmospheric turbulence[2,3] our research focuses on adaptive sampling within turbid water for depth measurement . Previous studies have explored TOF reconstruction in scattering media through phase frequency encoding[1] or efficient probing techniques.[4] However, such methods often rely on assumptions of minimal global illumination in the epipolar plane, an assumption that does not hold in heavily turbid underwater environments. Our approach utilizes a bistatic system, enabling effective reduction of global illumination through confocal imaging, a critical improvement for underwater applications.

MEMS Mirrors for Computer Vision: MEMS mirrors have found applications in diverse fields, from office automation to 360-degree displays.[5,6] While recent innovations have incorporated MEMS mirrors for controlling LiDAR transmitters in adaptive depth sensing,[7] our work extends this concept by controlling both the transmitter and receiver, adaptive principles from structured light systems to LiDARs[8,9]

Underwater LiDAR: While blue-green lasers have been used effectively in underwater LiDAR systems for shallow waters, turbidity significantly limits their efficacy.[10,11] Our bistatic confocal design aims to overcome these limitations, enhancing LiDAR's impact in underwater environments with scattering effects.

Scanning LiDAR: MEMS-modulated LiDAR systems have been deployed in various scenarios, including depth sensing and robotics.[12–16] Unique to our project is the placement of MEMS mirrors on both the transmitter and receiver, creating a bistatic system optimized for turbid environments and enabling foveated sensing.

Correspondence to jfolden@ufl.edu

NAVAIR Public Release SPR-2024-0202—Distribution Statement A: Approved for public release; distribution is unlimited.

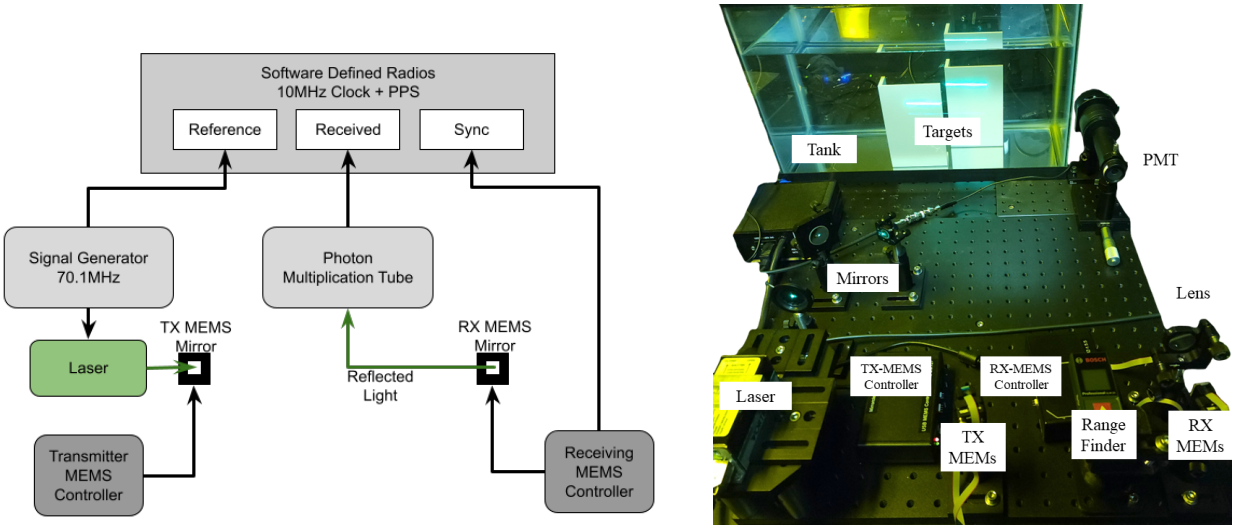

Figure 1. On the left, we show a block diagram of our prototype. The components that make up the prototype are a 514nm laser, a photomultiplier tube (PMT), three N200 software-defined radios, and two 3.6mm Mirrorcle MEMS mirrors. On the right, we show a labeled photo of our optical setup.

3. METHODOLOGY

In our setup shown in Fig. 1 we use two micro-electro-mechanical (MEMS) mirrors to control the transmitter and receiver directions for a lidar sensing through scattering media. There are pairs of voltages for each MEMS mirror, that physically rotate the mirror position into a desired angle. Let the azimuth and elevation angles for the receiver mirror be (ϕ_r, θ_r) and for the transmitter mirror be (ϕ_t, θ_t).

3.1 Bistatic Confocal MEMS-modulation

In this paper, by "confocal" we mean that the optical axes of the mirrors (i.e., the unit vector perpendicular to the mirror surface) always lie in the epipolar plane[17] (see Fig. 2). Therefore, one necessary (but not sufficient) constraint for mirror control is that they must satisfy the fundamental matrix $\mathbf{F}$. To use the fundamental matrix, consider a virtual image plane in front of each mirror, where the "pixel" corresponding to each mirror position is given by a corrected angle. For example, for the transmitter mirror we have pixels $x_t = [f\tan(\phi_t), f\tan(\theta_t)]$, where f is the virtual focal length of the virtual image plane such that the maximum and minimum extent of the pixels are $(\pm 1, \pm 1)$ respectively. Similarly, we also define x_r. The fundamental matrix constraint is $x_t^T \mathbf{F} x_r = 0$, which we recast in terms of MEMS mirror angles as:

$$[f\tan(\phi_t), f\tan(\theta_t)]^T \mathbf{F} [f\tan(\phi_r), f\tan(\theta_r)] = 0 \tag{1}$$

Successful signal reception in a clear medium aligns with the epipolar constraint point on the surface of the scene. However, in scattering media, received signals can occur at unintended locations along the epipolar line, potentially leading to depth misestimation. Our method addresses these challenges by detecting discontinuities along the ray and analyzing amplitude changes to accurately estimate depth even in dense scattering media.

3.2 Modulated Continuous-wave LiDAR

Our Continuous-wave (CW) LiDAR operates by modulating a laser with a reference signal $A_{ref}\cos(\omega + \chi_{ref})$ at the sensor, which is further modulated by the target's reflectance or scattering properties after reflecting off the first MEMS mirror. The received signal $A_{meas}\cos(\omega + \chi_{meas})$ is analyzed for the phase difference $\delta\chi = \|\chi_{meas} - \chi_{ref}\|$. Through phase unwrapping F_{unwrap}, this enables depth measurement as $Z = \frac{cF_{unwrap}(\delta\chi,\omega)}{2}$. Our focus also extends to the amplitude A_{meas} of the received signal, particularly in relation to scattering media.

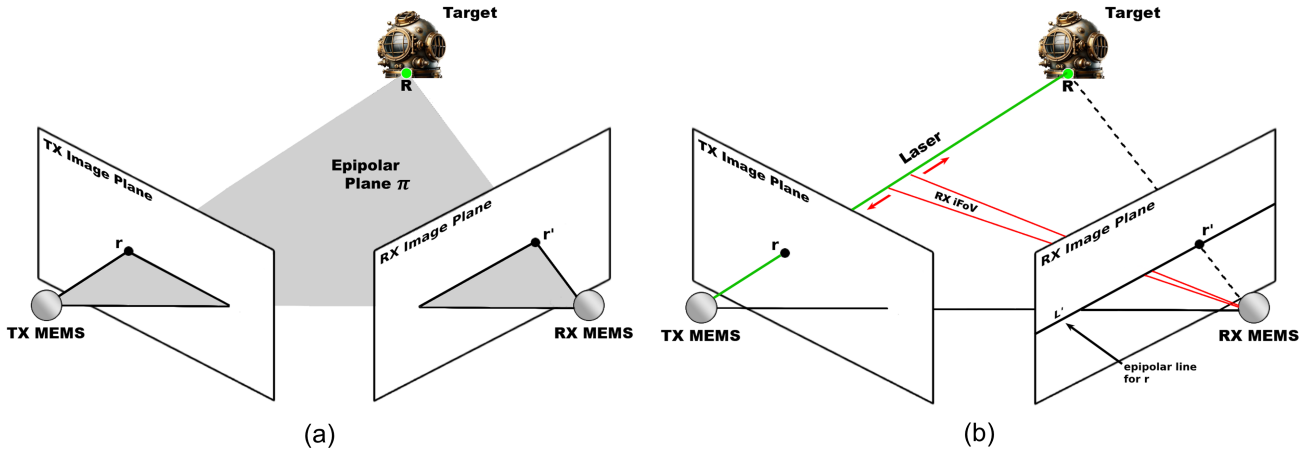

Figure 2. **Multi-view Geometry** The transmitter and receiver are indicated by the TX and RX MEMS, with their corresponding image planes. *(a)* The MEMS mirrors, 3D point $\mathbf{R}$, and its images $\mathbf{r}$ and $\mathbf{r}'$ lie in a common plane π. *(b)* The ray defined by TX and $\mathbf{r}$, ie. the laser, is imaged as a line L' in the RX image plane. The 3D point $\mathbf{R}$, which projects to $\mathbf{r}$, must lie along the ray, thus it must also lie on L'. We use the Epipolar line L' to scan the RX iFoV along the ray, capturing the reflected irradiance off the target and any backscatter off the ray. Figure inspired by a similar diagram in[17]

3.3 Relative Phase to Absolute Depth Calibration

Utilizing software-defined radios, we compare sinusoidal reference and received signals to calculate their relative phase $\delta\chi = \|\chi_{meas} - \chi_{ref}\|$. This phase difference, influenced by the oscillators' frequencies, allows us to measure relative depth, the variation in depth between measurements. However, this does not provide absolute depth, defined as the distance between the receiving MEMS and the laser target.

To convert relative phase measurements into absolute depth, we calibrate ground truth depth measurements with the phase differences. This process involves three planar experiments, using consistent transmitter sampling and depth measurements from the receiver MEMS with an adjacent hand-held laser rangefinder. By correlating these depth readings with phase differences, we create a linear regression model, effectively mapping relative phase to absolute depth.

4. RESULTS

In this section, we explore the advancements facilitated by our innovative system, as shown in Figure 3. This figure illustrates the system's impact on enhancing underwater imaging through dynamic depth sampling, where the LiDAR can dynamically adjust the iFOV in response to areas of interest. Through a series of comparative visual assessments, we reveal how the system's foveated sampling technique—powered by dual MEMS mirror-modulated components—substantially improves spatial detail in turbid water conditions. The visual evidence provided offers a clear narrative of the system's capabilities, underscoring the tangible benefits of our approach in underwater imaging.

4.1 Algorithmic Sampling and Foveation

Employing the fundamental matrix constraint (eq. 1), we generate receiver mirror angles for an in-depth amplitude profile creation. The measurements span an angular support volume ω_{rt}, defined by the azimuth and elevation intersections $(\phi_r, \theta_r) \cap (\phi_t, \theta_t)$. MEMS modulation allows comprehensive angular coverage within the sensor's field of view, allowing the receiver to traverse the epipolar line to compile a detailed amplitude profile $A_{meas}(\phi_r, \theta_r) \forall (\phi_t, \theta_t)$. This profile captures both scattered irradiance and target reflections, marked by discontinuities, thus enriching scene comprehension and range finding even under low visibility, as depicted in Fig. 3.

The significance of the foveation feature our system offers is clearly illustrated in Figure 3, where we elevate beyond the standard equiangular sampling approach of traditional LIDAR, i.e. sampling in all directions at the

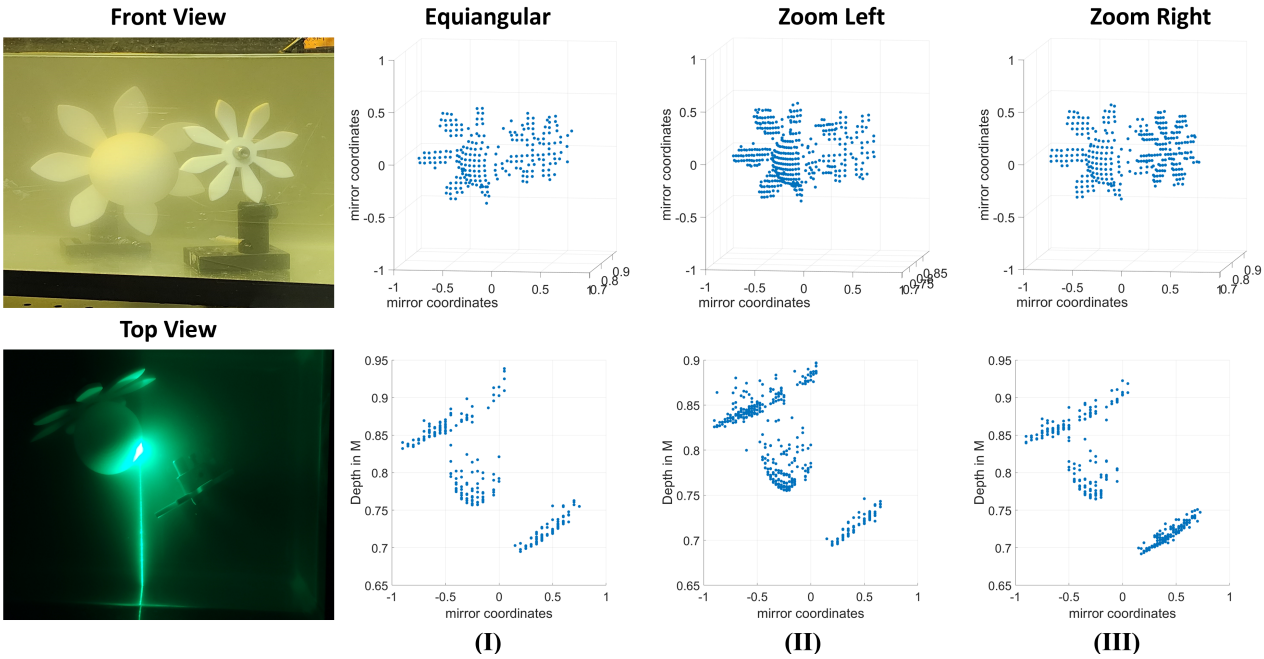

Figure 3. Demonstration of algorithmic sampling and foveation by our system, showcasing its "zoom" functionality on various objects within a turbid scene. Column (I) displays equiangular scanning across the entire scene. Columns (II) and (III) illustrate the system's ability to selectively zoom in: Column (II) focuses on the object to the left, while column (III) zooms in on the object to the right, highlighting the system's precise and adaptable foveation capabilities. The range of the scene is from 65cm to 1 meter.

same density. By judiciously controlling the MEMS mirrors to slow down over areas of interest, we enhance sampling resolution where it matters. The figure portrays this by intensifying the sample density on targeted objects—evident in the middle and right columns where the left and right objects, respectively, are examined with higher spatial resolution. This tailored sampling is critical, as it allows for detailed detection and analysis of objects in varying visibility conditions, significantly optimizing the performance of LIDAR in precision-critical applications such as autonomous navigation and detailed environmental mapping.

5. CONCLUSIONS AND LIMITATIONS

Conclusions: Our innovative bistatic adaptive LiDAR system demonstrates exceptional capability in confocal sampling and precise depth reconstruction, even under highly turbid conditions. By utilizing adaptive control coupled with a narrow iFOV on the receiver, our system adeptly captures both scene irradiance and scattered light. This dual capture, facilitated by the small iFOV and adaptive control, effectively creates a spatially-gated LiDAR engine. This engine can be utilized both during and after data acquisition to yield accurate depth reconstructions, demonstrating its versatility and effectiveness in challenging environments.

Limitations: The current prototype of our bistatic LiDAR system operates within a limited working volume, suitable for preliminary testing in controlled tank environments. This constraint is primarily due to the MEMS mirrors' maximum scanning angle of $\pm$ 7 degrees. One potential solution to expand the working volume is the incorporation of wide-angle lenses in front of the transmitter and receiver MEMS. Additionally, the limited reflective capacity of the 3.6mm MEMS mirror used as our receiver poses a challenge. The mirror's small size acts as a restrictive aperture, limiting the light reflected from the scene.

REFERENCES

[1] Gupta, M., Nayar, S. K., Hullin, M. B., and Martin, J., "Phasor imaging: A generalization of correlation-based time-of-flight imaging," *ACM Transactions on Graphics (ToG)* **34**(5), 156 (2015).

[2] Beckers, J. M., "Adaptive optics for astronomy: principles, performance, and applications," *Annual review of astronomy and astrophysics* **31**(1), 13–62 (1993).

[3] Tyson, R. K., [*Principles of adaptive optics*], CRC press (2015).

[4] O'Toole, M., Heide, F., Xiao, L., Hullin, M. B., Heidrich, W., and Kutulakos, K. N., "Temporal frequency probing for 5d transient analysis of global light transport," *ACM Transactions on Graphics (ToG)* **33**(4), 87 (2014).

[5] Raskar, R., Welch, G., Cutts, M., Lake, A., Stesin, L., and Fuchs, H., "The office of the future: A unified approach to image-based modeling and spatially immersive displays," in [*Proceedings of the 25th annual conference on Computer graphics and interactive techniques*], 179–188, ACM (1998).

[6] Jones, A., McDowall, I., Yamada, H., Bolas, M., and Debevec, P., "Rendering for an interactive 360 degree light field display," in [*SIGGRAPH*], ACM (2007).

[7] Tasneem, Z., Wang, D., Xie, H., and Koppal, S. J., "Directionally controlled time-of-flight ranging for mobile sensing platforms," in [*Robotics: Science and Systems XIV*], (2018).

[8] Narasimhan, S. G., Nayar, S. K., Sun, B., and Koppal, S. J., "Structured light in scattering media," in [*Tenth IEEE International Conference on Computer Vision (ICCV'05) Volume 1*], **1**, 420–427, IEEE (2005).

[9] Achar, S., Bartels, J. R., Whittaker, W. L., Kutulakos, K. N., and Narasimhan, S. G., "Epipolar time-of-flight imaging," *ACM Transactions on Graphics (TOG)* **36**(4), 37 (2017).

[10] Akkaynak, D. and Treibitz, T., "Sea-thru: A method for removing water from underwater images," in [*Proceedings of the IEEE/CVF conference on computer vision and pattern recognition*], 1682–1691 (2019).

[11] Berman, D., Levy, D., Avidan, S., and Treibitz, T., "Underwater single image color restoration using haze-lines and a new quantitative dataset," *IEEE transactions on pattern analysis and machine intelligence* **43**(8), 2822–2837 (2020).

[12] Flatley, T. P., "Spacecube: A family of reconfigurable hybrid on-board science data processors," (2015).

[13] Stann, B. L., Dammann, J. F., Del Giorno, M., DiBerardino, C., Giza, M. M., Powers, M. A., and Uzunovic, N., "Integration and demonstration of mems–scanned ladar for robotic navigation," in [*Proc. SPIE*], **9084**, 90840J (2014).

[14] Krastev, K. T., Van Lierop, H. W., Soemers, H. M., Sanders, R. H. M., and Nellissen, A. J. M., "Mems scanning micromirror," (Sept. 3 2013). US Patent 8,526,089.

[15] Milanović, V., Kasturi, A., Yang, J., and Hu, F., "A fast single-pixel laser imager for vr/ar headset tracking," in [*Proc. of SPIE Vol*], **10116**, 101160E–1 (2017).

[16] Milanović, V., Kasturi, A., Siu, N., Radojičić, M., and Su, Y., ""memseye" for optical 3d tracking and imaging applications," in [*Solid-State Sensors, Actuators and Microsystems Conference (TRANSDUCERS), 2011 16th International*], 1895–1898, IEEE (2011).

[17] Hartley, R. and Zisserman, A., [*Multiple view geometry in computer vision*], Cambridge university press (2003).